Arch. Metall. Mater. **69** (2024), 2, 535-540

DOI: https://doi.org/10.24425/amm.2024.149780

V.M. CALINESCU[1], M. OPROESCU[2], V.G. IANA[2], C.M. DUCU[3], A.-G. SCHIOPU[3*]

MORPHOLOGICAL CHANGES OF METAL OXIDES THROUGH THE SOLAR PHYSICAL VAPOR DEPOSITION PROCESS

The paper brings to the attention of researchers the morphological changes of metal oxides, which appear as a result of the process of physical solar vapor deposition (SPVD) based on experiments carried out at the CNRS-PROMES laboratory, UPR 8521, belonging to the French National Centre for Scientific Research (CNRS). The SPVD process is an innovative tool who has been developed in 2 kW solar furnaces at Odeillo-Font Romeu, France, to synthesis pure and doped nanoparticles, such as: ZnO, CeO_2, ZrO_2, BiO_2, SiO. A variety of metal oxides nanoparticles have been obtained by focusing solar energy on pellets of commercial powders through the controlled process of vaporization followed by condensation directed on a cooper tube or on nanoporous filter. After the micrograph analysis the change of shape and dimension can be observed depending on the type of oxide and the process parameters. It is noticed the appearance of new morphologies, not found in other synthesis methods. The paper brings new information about morphological and dimensional changes after synthesis by physical process which can be essential for researchers, in the choice of methods for the elaboration of nanomaterials.

Keyword: Nanoparticles; Morphology; Image analysis; Physical vapor deposition

1. Introduction

The global nanomaterials market was valued at more than $8 trillion in 2022 and is expected to grow continuously as key factors influencing market growth include government funding and strategic partnerships [1]. In general, conventional materials have grains in size from 100 microns to a few millimeters and contain several million atoms each. A nanocrystalline material has grains with sizes between 1-100 nm. Dimensional, to 1 nanometer corresponding between 3-5 atoms, depending on the radius of the atom. Thus, we can say that nanometric grains contain only about 500 atoms each. As the grain size decreases, there is a significant increase in the number of grains and interphases in the volume fraction. For a size of about 5 nm, almost 50% of the volume is represented by the grain boundaries. Interfaces, dislocations, compositional heterogeneities are governed in these structures of nanometric size. The increase in the specific surface of the grain, along with its decrease in size and the increase in the number of grain boundaries, influence the chemical, physical and biological properties of the material. The electronic levels of the nanomaterials cause changes in the optical and electrical properties, when the size of the grains approaches the molecular size ($d < 5$ nm).

Metal oxide nanoparticles are an important class of nanomaterials that have initiate several uses in science and technology. Metal oxide nanoparticles shows special optical and electronic properties different from bulk materials. They are widely exploited due to their properties: catalyst in diesel fuels to improve emission quality [2], sensors [3], ceramic applications [4], medical treatments [5], antitumor agents [6], antibacterial agents [7,8] or solar cells [9]. The scientific interest in nanomaterials is explained by the fact that all properties (physical and chemical) change when the particle approaches nanometric dimensions [10-12].

Current research focuses on understanding phenomena at the nanometric scale, in order to create and use systems and structures that have new properties and functions, different from those of conventional materials. Among the synthesis methods of these nanoparticles, the chemical methods present the advantage of versatility, obtaining large quantities [13-16], while the physical methods present the advantage that the formation of agglomerations in nanopowders can be avoided [17-19].

[1] DOCTORAL SCHOOL MATERIALS SCIENCE AND ENGINEERING, NATIONAL UNIVERSITY OF SCIENCE AND TECHNOLOGY POLITEHNICA BUCHAREST, SPLAIUL INDEPENDENTEI, NO. 313, SECTOR 6, BUCHAREST, ROMANIA
[2] PITEȘTI UNIVERSITY CENTRE, FACULTY OF ELECTRONICS, COMMUNICATION AND COMPUTERS, NATIONAL UNIVERSITY OF SCIENCE AND TECHNOLOGY POLITEHNICA BUCHAREST , TARGU DIN VALE, NO.1, PITESTI, ROMANIA
[3] PITEȘTI UNIVERSITY CENTRE, FACULTY OF MECHANICS AND TECHNOLOGY, NATIONAL UNIVERSITY OF SCIENCE AND TECHNOLOGY POLITEHNICA BUCHAREST, TARGU DIN VALE, NO.1, PITESTI, ROMANIA

* Coressponding author: gabriela.schiopu@upb.ro

Currently, researchers believe that in order to obtain superior properties, it is necessary to obtain nanocrystalline structures, control the grain size and the nucleation processes. Physical Vapor Deposition (PVD) methods are mainly based on the principle of evaporation and/or sputtering, of solid-state material on a base material. In general, the PVD process is used to obtain coatings in the form of thin layers, with optical, electrical, anticorrosive or decorative properties [20]. However, at the same time, the process can also be used to obtain powders with nanometric dimensions, if the process is strictly controlled from the point of view of pressure, working temperature and the way of making the deposition. In this study, we report on morphological modification of some metal oxides elaborated through SPVD (Solar Physical Vapor Deposition) started from commercial precursors, easy to procure [17,18]. The results obtained will provide an important key to develop new methods of synthesis of nanoparticles with new morphologies.

2. Experiment

Concentrated solar energy is a potential source of energy for developing new nanomaterials and solar furnaces are research installations develop in France, Spain, Germany, Turkey, Italy. The furnace is an assemblage of curved mirrors or mirrored surfaces that capture the sun rays and reflect them to a single point where the energy is concentrated. With some solar furnaces, this focused energy can reach a temperature of 4000°C. The largest solar furnance is located in Font-Romeu-Odeillo-Via.

The Odeillo Four Solaire has a height of 50 m, a length of 60 m and a width of 30 m, comprising 63 heliostats. The entire structure is powered by solar energy and has been operating since 1969. As a result of its thermal power of one megawatt, it can reach temperatures of 3300°C, which is nearly 10.000 times what the sun can produce.

The physical synthesis of nanostructured powders under solar energy were used for metal oxides synthesis such as: ZnO, TiO_2, CeO_2, Bi_2O, CuO, MnO, SnO, In_2O.

The nanopowders synthesis process of cooper oxide, zinc oxide and manganese oxide, pure or doped, takes place in 3 stages:

- In the first stage, the pressed commercial powder is exposed to solar radiation and evaporated inside the solar reactor. The solar flux must meet the condition of being greater than 800 W/m^2 to ensure evaporation and not melting of the precursor capsule.
- In the second stage, condensation of the evaporated phases takes place on the cooper support continuously cooled with water, positioned above in the glass reactor, as well as on the ceramic nanoporous filter under suction pressure.
- In the third stage, the dust is collected from the copper support and from the nanoceramic filter.

The process takes place under solar radiation, characterized by solar radiation flow and under pressure. The experimental conditions are presented in TABLE 1.

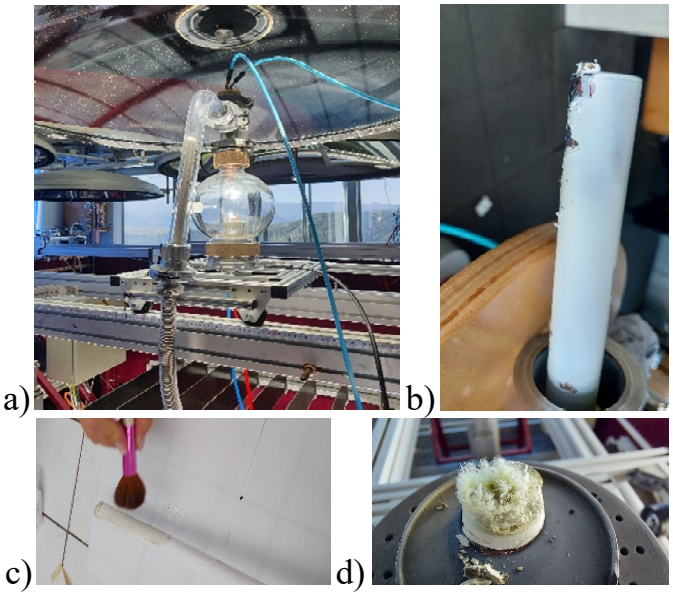

Fig. 1. Experimental steps a) Solar reactor during the synthesis, b) Copper support coated by powder c) Powder collection on the ceramic filter, d) Target after vapor condensation

TABLE 1

Experimental parameters of SPVD experiments

Sample	Solar Flow (W/m^2)	Pressure (barr)
VcCuO	1020	$10*10^{-2}$
Vc10MnCuO	933	$5*10^{-2}$
VcZnO	980	$2,6*10^{-2}$
Vc10AlZnO	853	$7,9*10^{-2}$
VcMnO	1015	$5*10^{-2}$
Vc2.5ZrMnO	830	$8*10^{-2}$

After collecting the powders, they are morphologically analyzed by electron microscopy [21]. The dimensional analysis of the particles identified by types of morphologies is performed with the Image J software [22-24].

3. Results and discussion

3.1. Morphological analysis of the powders

Electron micrographs highlight the shape of the powder particles before and after the SPVD process. The micrographs are shown in Fig. 2. Obviously, the controlled vaporization process under solar radiation changes the morphology. To the same point, the doping element Al, Mn or Zr, as the case may be, totally changes the morphology compared to the non-doped powders. Fig. 2 shows the morphologies of precursors and collected powders after SPVD process.

The first oxide studied is copper oxide. The SEM micrographs made on the commercial powder, used as a precursor, in the form of a tablet, highlight the irregular shape of the pellets, present in the form of agglomerations (Fig. 2a). After the synthesis process under solar flux, a change in morphology can

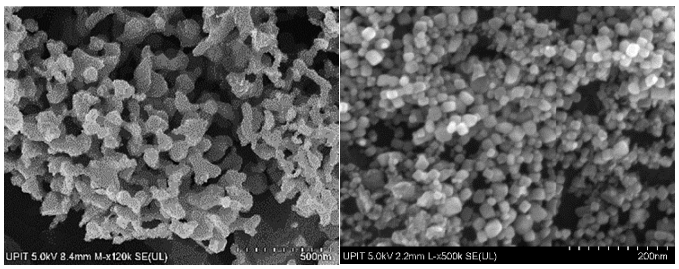
a) CuO com. b) VcCuO

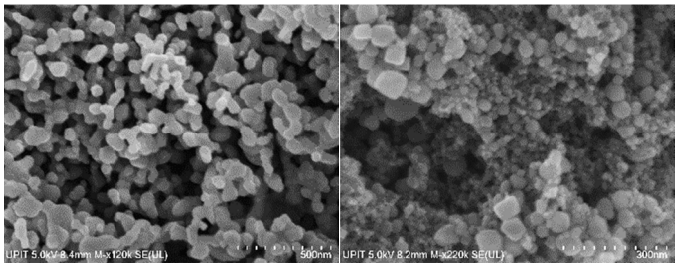
c) 10MnCuO com. d) Vc10MnCuO

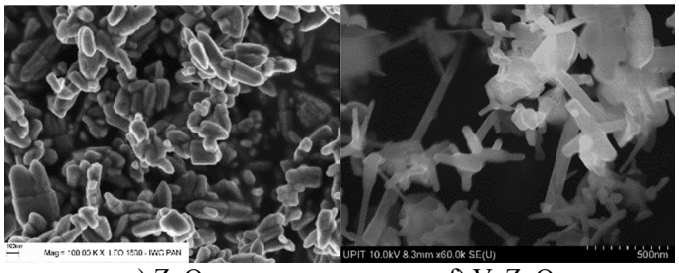
e) ZnO com. f) VcZnO

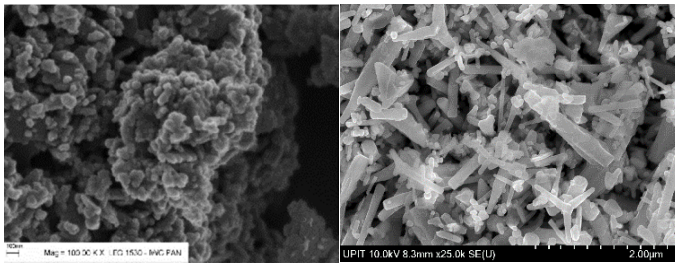
g) 10AlZnO com. h)Vc10AlZnO

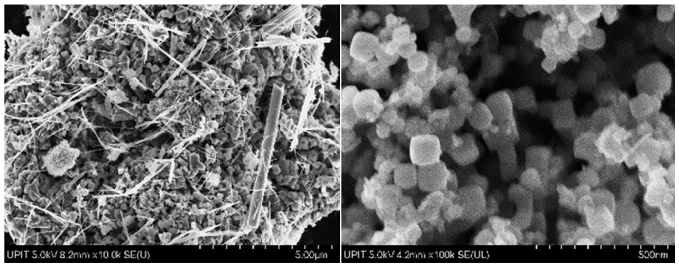
i) MnO com. j)VcMnO

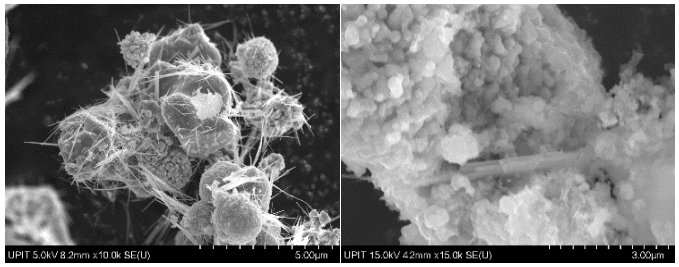
k) 2.5ZrMnO com. l) Vc2.5ZrMnO

Fig. 2. Micrographs of a) c) e) g) i) k) commercial powders and b) d) f) h) j) l) micrographs of nanoparticles after SPVD process

be observed. The particles acquire a polyhedral shape, without agglomeration (Fig. 2b). In the case of Mn doping, the morphology of the precursor powders does not differ from that of the non-doped powders (Fig. 2c). And in the case of vapor-condensed powders, the morphology is also polyhedral (Fig. 2d).

The second precursor is zinc oxide which is characterized by a pellet type morphology, specific to chemical syntheses (Fig. 2e). Spectacularly, after vapor condensation, the morphology changes becoming tetrapods (whiskers) and polyhedral particles as shown in fig. 3f, which highlights that not all particles have been transformed. If the zinc oxide presents as Al dopant ion, in its commercial state, it also has the form of agglomerated pellets (Fig. 2g). This shape changes after SPVD to whiskers, cylinders and polyhedral particles. (Fig. 2h).

The third commercial manganese oxide is characterized by agglomerated particles, cylindrical type, wire type and irregular polyhedral particles (Fig. 2i). After SPVD, the morphology settles to a polyhedral shape, without agglomerations (Fig. 2j). Doping with Zr causes an agglomerated, ball-type morphology of polyhedra fixed by wires (Fig. 2k). The agglomeration is preserved even after SPVD, the polyhedral particles with several cylinders becoming predominant (Fig. 2l).

3.2. Dimensional analysis of particles

Particles from each micrograph before and after SPVD process were dimensional measure using Image J software. The total number of analyzed particles is presented in TABLE 2.

TABLE 2

Number of analyzed particles

Sample	Number of analyzed particles	Sample	Number of analyzed particles
CuO com.	46	VcCuO	57
10MnCuO com.	79	Vc10MnCuO	77
ZnO com.	27	VcZnO	40
10AlZnO com.	72	Vc10AlZnO	108
MnO com.	96	VcMnO	108
2.5ZrMnO com.	69	Vc2.5ZrMnO	66
Total	389	Total	443

The first oxide, cooper oxide, present pellets with a size that varies from to 42 to 114 nm. The dimensional distribution of the particles is shown in the Fig. 3a which highlights a dimensional non-uniformity. The majority are particles with a size between 52 and 98 nm. After SPVD process the dimension of polyhedral particles obtained decrease to 8 up to 45 nm. The dimensional distribution of the 57 measured particles is shown in the Fig. 3b.

The commercial copper oxide particles doped with Mn have polyhedral shapes with sizes between 28 and 137 nm. The evaporation and condensation process reduces the size to 15 nm. The largest measured particle reaches 89 nm. The distribution of particles is shown in Fig. 4.

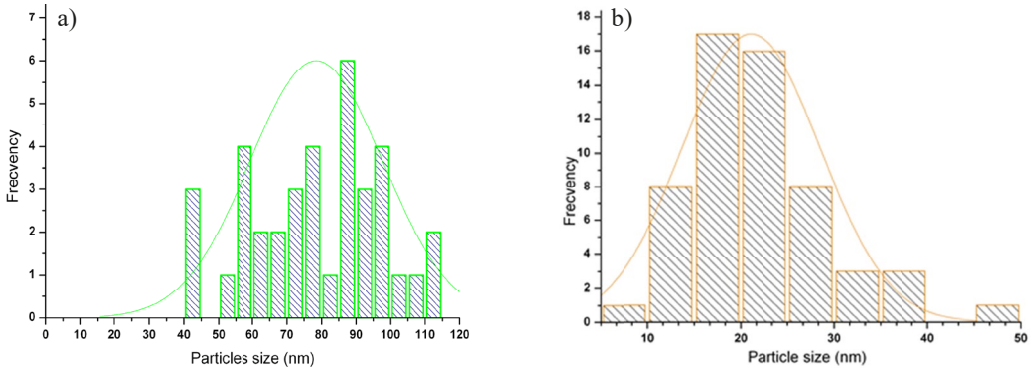

Fig. 3. a) Particle size distribution histogram of CuO com, b) Particle size distribution histogram of VcCuO

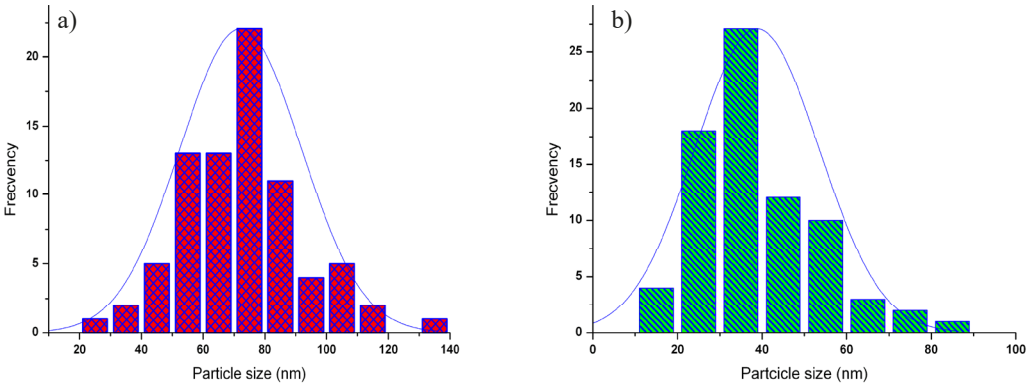

Fig. 4. a) Particle size distribution histogram of 10MnCuO, b) Particle size distribution histogram of Vc10MnCuO

The size of the second oxide, represented by 27 measured pellets zinc oxide varies from 65 to 287 nm, with a homogeneous distribution between 75 and 175 nm, shown in Fig. 5a. The sizes of the whiskers after SPVD vary from 53 to 270 nm while the remaining untransformed particles vary from 47 to 337 nm, due to agglomeration process. Their distribution is shown in Fig. 5b.

In the case of Al-doped zinc oxide, particles have a pellet size between 35 and 282 nm, with uniform distribution between 61 and 87 nm Fig. 6a). The whiskers obtained after SPVD have sizes starting from 247 to 709 nm, and the identified cylinders have an average length of 950 nm. The 61 measured polyhedral particles have a uniformly normalized distribution shown in Fig. 6b.

The complex morphology of commercial manganese oxide contains: polyhedral particles with dimensions between 197 and 552 nm, cylinders with an average length of 2.82 µm, as well as wires with an average length of approximatively 1 µm. The polyhedral manganese oxide particles, obtained after SPVD, have sizes that vary from 36 to 138 nm, with a frequency shown in the Fig. 7a.

The polyhedral particles of precursor manganese oxide doped with Zr have sizes from 146 to 294 nm (Fig. 7b.), and the wires that keep these particles agglomerated have an average length of 1.1 µm. The solar process modifies the dimensions, such as the polyhedral particles become between 118 and 481 nm, whose distribution is presented in Fig. 8a, while the newly appeared morphology, the cylindrical one has an average length of 1.7 µm with a uniform distribution like in Fig. 8b.

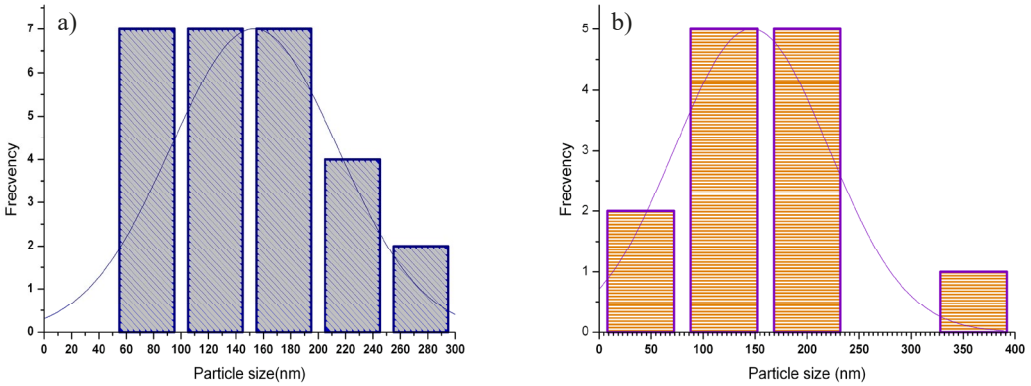

Fig. 5. a) Particle size distribution histogram of ZnO, b) Particle size distribution histogram of VcZnO

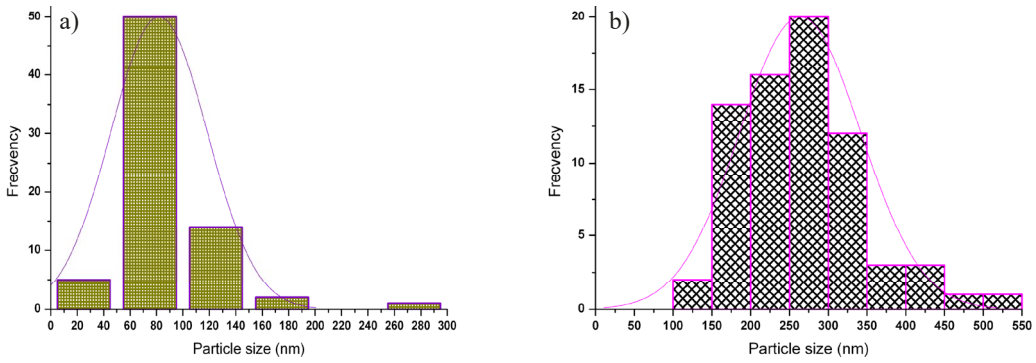

Fig. 6. a) Particle size distribution histogram of 10AlZnO, b) Particle size distribution histogram of Vc10AlZnO

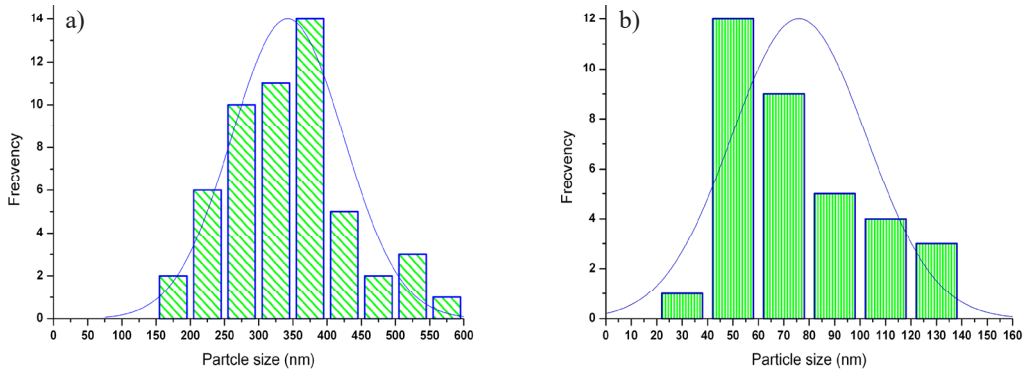

Fig. 7. a) Particle size distribution histogram of MnO com, b) Particle size distribution histogram of Vc MnO

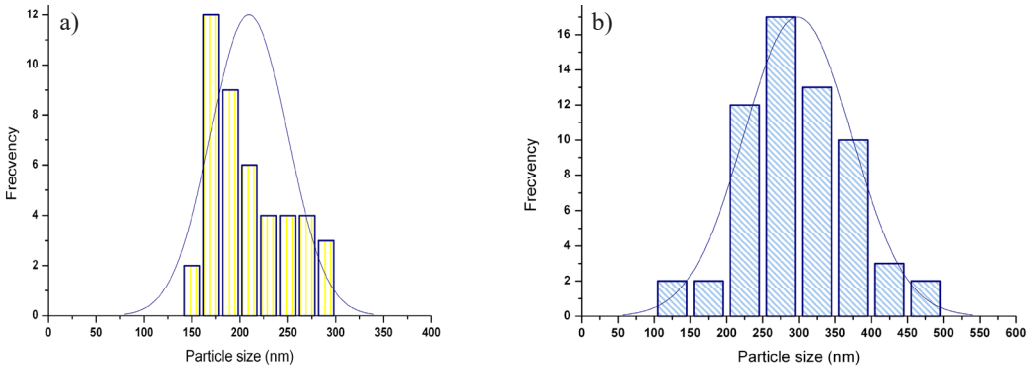

Fig. 8. a) Particle size distribution histogram of 2.5ZrMnO com, b) Particle size distribution histogram of Vc 2.5ZrMnO

4. Conclusions

Several types of nanopowders were prepared to highlight the influence of the SPVD process on the morphology and particle sizes. A total of 832 nanoparticles in 12 electron micrographs were analyzed. Morphologies and size of each form of particle were studied, and the following conclusions result:

(1) after controlled vaporization under solar flux and condensation on cold elements the morphology undergoes important changes;
(2) the presence of dopant modifies the morphology and particle size in commercial state and also after SPVD process;
(3) the decrease of particle size after SPVD process is due to the physical vaporization and controlled condensation process of obtaining nanoparticles;
(4) a radical change in morphology is evident in the case of zinc oxide, when after SPVD the whiskers type morphology is formed;
(5) cooper oxide and manganese oxide predominantly show polyhedral particles both in the precursor state and after the vapor condensation process;
(6) in the commercial state, the distribution of polyhedral particles or pellets is uniform, while after the SPVD process, due to the morphological complexity, the distribution varies depending on the shape of the particles.

Acknowledgments

This project has received funding from the European Union's Horizon 2020 research and innovation programme under grant agreement No 823802. We

thank the CNRS-PROMES laboratory, UPR 8521, belonging to the French National Centre for Scientific Research (CNRS) for providing access to its installations, the support of its scientific and technical staff, and the financial support of the SFERA-III project (Grant Agreement No 823802).

REFERENCES

[1] Nanomaterials Market Share, Size, Trends, Industry Analysis Report, By Application (Aerospace, Automotive, Medical, Energy & Power, Electronics, Paints & Coatings, Others), By Product; By Region; Segment Forecast, 2022-2030, Report ID: PM2239, (2021).

[2] I.V. Yentekakis, D.P Gournis, M.A Karakassides, Nanomaterials in Catalysis Applications. Catalysts **13**, 627, (2023). DOI: https://doi.org/10.3390/catal13030627

[3] D. Lun, K. Xu, Recent Progress in Gas Sensor Based on Nanomaterials. Micromachines (Basel). Jun 10, **13** (6), 919 (2022). DOI: https://doi.org/10.3390/mi13060919. PMID: 35744533; PMCID: PMC9229305

[4] S.C. Thomas Harshita, P.K. Mishra, S. Talegaonkar, Ceramic Nanoparticles: Fabrication Methods and Applications in Drug Delivery. Curr Pharm Des. **21** (42), 6165-88 (2015). DOI: https://doi.org/10.2174/1381612821666151027153246. PMID: 26503144

[5] P. Daisy, K. Saipriya, Biochemical analysis of Cassia fistula aqueous extract and phytochemically synthesized gold nanoparticles as hypoglycemic treatment for diabetes mellitus. International Journal of Nanomedicine **7**, 1189-1202 (2012). DOI: https://doi.org/10.1142/S0218625X19502196

[6] M.P. Vinardell, M. Mitjans, Antitumor Activities of Metal Oxide Nanoparticles. Nanomaterials **5**, 1004-1021, (2015).

[7] M.S Chavali, M.P. Nikolova, Metal oxide nanoparticles and their applications in nanotechnology. SN Appl. Sci. **1**, 607 (2019). DOI: https://doi.org/10.1007/s42452-019-0592-3

[8] A.M. Negrescu, M.S. Killian, S.N.V. Raghu, P. Schmuki, A. Mazare, A. Cimpean, Metal Oxide Nanoparticles: Review of Synthesis, Characterization and Biological Effects. J. Funct. Biomater. **13**, 274 (2022). DOI: https://doi.org/10.3390/ jfb13040274

[9] N. Kumar, M. Kalyan Phani, P. Chamoli, M.K. Manoj, A. Sharma, W. Ahmed, A. Kumar Srivastava, S. Kumar, Emerging Nanotechnologies for Renewable Energy, Chapter 10 – Nanomaterials for advanced photovoltaic cells, Micro and Nano Technologies 239-258 (2021). DOI: https://doi.org/10.1016/B978-0-12-821346-9.00006-7

[10] S. Iravani, H. Korbekandi, S.V. Mirmohammadi, B. Zolfaghari, Synthesis of silver nanoparticles: chemical, physical and biological methods. Res Pharm Sci. **9** (6), 385-406 (2014). PMID: 26339255; PMCID: PMC4326978.

[11] A. Ali, H. Zafar, M. Zia, Ul Haq I, A.R. Phull, J.S. Ali, A. Hussain, Synthesis, characterization, applications, and challenges of iron oxide nanoparticles. Nanotechnol. Sci. Appl. **9**, 49-67 (2016). DOI: https://doi.org/10.2147/NSA.S99986

[12] A.S.H. Makhlouf, Current and advanced coating technologies for industrial applications in Nanocoatings and Ultra-Thin Films, 2011, A volume in Woodhead Publishing Series in Metals and Surface Engineering, book.

[13] N. Jain, A. Bhargava, S. Majumdar, J.C. Tarafdar, J. Panwar, Extracellular biosynthesis and characterization of silver nanoparticles using Aspergillus flavusNJP08: A mechanism perspective. Nanoscale **3** (2), 635-41 (2010). DOI: https://doi.org/10.1039/c0nr00656d

[14] G. Calin, L. Sachelarie, N. Olar, Influence of Synthesis Conditions on the Chemical Stru,cture and Composition of ZnO Nanoparticles Composite Systems / Polymer Fibers. Arch. Metall. Mater. **67**, 2, 601-606 (2022). DOI: https://doi.org/10.24425/amm.2022.137796

[15] M. Gizowska, I. Kobus, K. Perkowski, M. Piątek, G. Konopka, I. Witosławska, M. Osuchowski, Size and morphology of yttria nanopowders obtained by solution combustion synthesis. Arch. Metall. Mater. **63**, 2, 743-748 (2018). DOI: https://doi.org/10.24425/122400

[16] L.M. Cursaru, A.G. Plaiasu, C.M. Ducu, R.M. Piticescu, I.A. Tudor, Carbon Nanotube/Polyaniline Composite Films Prepared by Hydrothermal-Electrochemical Method for Biosensor Applications, 2018 International Semiconductor Conference (CAS), 249-252.

[17] A.G. Plăiașu, M.C. Ducu, S.G. Moga, A.D. Negrea, E.M. Modan, Nanostructured transition metal oxides obtained by SPVD, Manufacturing Rev., **7**, 12 Special Issue – The emerging materials and processing technologies, (2020). DOI: https://doi.org/10.1051/mfreview/2020009

[18] A.G. Plaiasu, C.M. Topala, A. Dinu, M. Abrudeanu, C. Sutan, Copper Oxides Nanopowders Synthesis by SPVD and Characterization. Revista de Chimie **66** (10), 1636-1638 (2015).

[19] M. Stanciulescu, M. Abrudeanu, C. Ducu, A.G. Plaiasu, Chemical Redistribution and Microstructural Evolution of ODS Fe-Cr Powders During Mechanical Alloying. Revista de Chimie **69** (2), 495-498 (2018).

[20] L. D'Avico, R. Beltrami, N. Lecis, S.P. Trasatti, Corrosion Behavior and Surface Properties of PVD Coatings for Mold Technology Applications. Coatings **9**, 7, (2019). DOI: https://doi.org/10.3390/coatings901000

[21] Nanoparticle Technology Handbook, Basic Properties and Measuring Methods of Nanoparticles,\ 3-47, (2018), https://www.sciencedirect.com/science/article/pii/B9780444641106000019

[22] John G. Walker, Nam Trung Huynh, Rui Chen, Image vector histogram approach to nanoparticle sizing, Appl. Opt. **51**, 651-658, (2012).

[23] J. Gabriela Calvillo-Vázquez, Hugo A. Guillén-Ramírez, Melis, sa DiazDuarte-Rodríguez, Angel Licea-Claverie, Eugenio R. Méndez, Particle size distribution from extinction and absorption data of metallic nanoparticles, Appl. Opt. **58** (36), 9955-9966 (2019).

[24] Chapter 1 – Basic Properties and Measuring Methods of Nanoparticles, Editor(s): Makio Naito, Toyokazu Yokoyama, Kouhei Hosokawa, Kiyoshi Nogi, Nanoparticle Technology Handbook (Third Edition), Elsevier 3-47, (2018). DOI: https://doi.org/10.1016/B978-0-444-64110-6.00001-9; ISBN 9780444641106